metals

MDPI

Article

Study on the Preparation and Performance of Low-Temperature Sintering and High-Thermal-Conductivity Silver Nanowire Film

Yongqian Peng, Yicong Ye *, Cuijuan Yu, Zhen Wang, Yuanxi Xu and Yongguo Du

College of Aerospace Science and Engineering, National University of Defense Technology, Changsha 410073, China; chrisyq_peng@163.com (Y.P.)
* Correspondence: yeyicongde2021@163.com

Abstract: This paper proposes a new silver nanoscale joining material, silver nanowire film, as an alternative joining approach for high-power and large-size chip packaging. The silver nanowire film was prepared by pressing filtration with silver nanowire that was synthesized using the polyol method. We found that the tensile strength of the film reached 3.40 MPa and the content of the silver reached up to 99.0 wt%. This paper further studies the influence of the size of silver nanowires on the performance of silver nanowire film. The experimental results show that the silver nanowire films prepared with silver nanowires with longer lengths and smaller diameters displayed better performances. The silver nanowire film with the best performance was prepared using silver nanowire with a diameter of 88 nm and a length of 29 μm. The thermal resistance of the sintered silver nanowire film that was hot-pressed at 250 °C 10 MPa was only 1.28 $K \cdot W^{-1}$. The shear strength of the sintered joint was 56.4 MPa, and the fracture that occurred in the sintered silver nanowire film displayed a good plasticity.

Keywords: electronic packaging; nano-silver; low-temperature sintering; shear strength; high thermal conductivity

Citation: Peng, Y.; Ye, Y.; Yu, C.; Wang, Z.; Xu, Y.; Du, Y. Study on the Preparation and Performance of Low-Temperature Sintering and High-Thermal-Conductivity Silver Nanowire Film. *Metals* **2023**, *13*, 819. https://doi.org/10.3390/met13040819

Academic Editor: Alain Pasturel

Received: 14 March 2023
Revised: 18 April 2023
Accepted: 18 April 2023
Published: 21 April 2023

1. Introduction

In order to conduct more complex and diversified tasks and achieve a faster computing speed and lighter volume, electronic devices continue to be developed with the aim of developing high power [1]. However, with the miniaturization and high performance of such electronic devices, their heat flux is becoming increasingly higher; sometimes, the heat flux part may even reach 40 kW/cm^2 [2]. A large number of studies have shown that a high temperature will limit the performance of semiconductor chips and seriously harm the reliability of electronic devices; more than 60% of all failures of electronic devices are caused by the overheating of interconnecting materials of electronic packaging [3]. Heat dissipation has become the bottleneck of the development of high-power electronic devices, which puts forward higher requirements for the packaging materials of electronic devices [4,5].

Currently, Sn-Pb solder is the most widely used material in micro-electronic joining; this solder has a good strength and low cost, but gradually, its low melting point, environmental pollution, and low thermal conductivity make it fail to meet the requirements of high-power electronic device packaging [6–8]. Silver nanoscale materials are potential materials for micro-electronic joining [9]. On the one hand, bulk silver has a melting point of up to 961 °C, which can well avoid the remelting of solder during the working process of a device, thus significantly increasing the reliability of electronic devices. At the same time, due to the small size effect of the nanoscale, the sintering temperature of silver nanoscale materials is much lower than that of bulk silver [10–12]. Therefore, silver nanoscale materials have the characteristics of low-temperature sintering and a

high-temperature service. On the other hand, benefiting from the ultra-high thermal conductivity of bulk silver (429 $W \cdot m^{-1} \cdot K^{-1}$), sintered silver nanoscale materials also have an excellent thermal conductivity, although there are pores and remains that reduce their thermal conductivity [13,14]. For example, Zhang et al. [15] reported that nanoscale silver paste prepared from silver nanoparticles with a diameter of about 110 nm has a thermal conductivity of up to 247 $W \cdot m^{-1} \cdot K^{-1}$ after hot-pressing, which is five times that of the traditional Sn-Pb solder. In addition, the good mechanical properties of silver also provide a higher reliability for electronic packaging. As reported by Thomas et al. [16], the shear strength of the copper–silver–copper joints can reach 45 MPa. Therefore, silver nanoscale material is almost the most suitable for high-power electronic device joining.

According to the existing reports, silver nanoscale joining material is mainly in the form of a paste; it is usually prepared from silver nanoparticles by adding organic polymers, of which the silver nanoparticles are the key to their performance, while organic polymers can prevent nanoparticle aggregation and regulate the rheological properties of the paste [17–19]. This material usually requires dispensing or screen-printing, which leads to its application to chips with small sizes only [20]. At the same time, due to the addition of more organic polymers, the sintering process will be complex and the carbon will be left behind, which significantly increases the cost and reduces the thermal conductivity [21]. In this study, a silver nanoscale joining material called silver nanowire film was proposed. It is made from silver nanowires by pressure filtration and drying, for which the preparation process is simple and has a low organic content. In addition, silver nanowire film looks similar to a sheet and it has a degree of strength so that it can be cut, which is suitable for joining large-size chips. This paper also studied the influence of different diameters and lengths of silver nanowires on the performance of silver nanowire film.

2. Materials and Methods

2.1. Preparation of Silver Nanowire Film

The silver nanowires were synthesized by the polyol method. First, $AgNO_3$ and PVP (polyvinyl pyrrolidone, K60, Beijing Hengchengxingsheng Technology, Co., Ltd., Beijing, China) glycol and NaCl glycol solutions were pre-prepared, respectively. Then, 1.6 L of PVP solution, 0.16 L of NaCl solution, and 4.8 L of EG (ethylene glycol) were added into the reactor. $AgNO_3$, NaCl, and EG were purchased from Shanghai Aladdin Biochemical Technology Co., Ltd. After raising to the target temperature, 1.6 L of $AgNO_3$ solution was added, the reaction was stopped after holding for 4 h, and, finally, the silver nanowire solution was obtained after cooling. In order to study the influence of silver nanowires with different diameters and lengths on the performance of silver nanowire film, five kinds of silver nanowires with different lengths and diameters were synthesized, and these five kinds of silver nanowires were used to prepare five kinds of silver nanowire films. The length and diameter of the silver nanowires were measured and counted using Image Pro Plus. SEM (MIRA4 LMH, Tescan, Brno, Czech Republic) images of five kinds of silver nanowires and their size statistics are shown in Figure 1. All synthetic formulas are shown in Table 1.

Table 1. Synthetic formulas of different sizes of silver nanowire.

NO	c ($AgNO_3$)/M	c (PVP)/M	c (NaCl)/mM	Temperature/°C
1	0.3	1.00	8	120
2	0.3	0.5	8	120
3	0.2	1.00	8	130
4	0.2	1.00	10	140
5	0.4	0.75	8	110

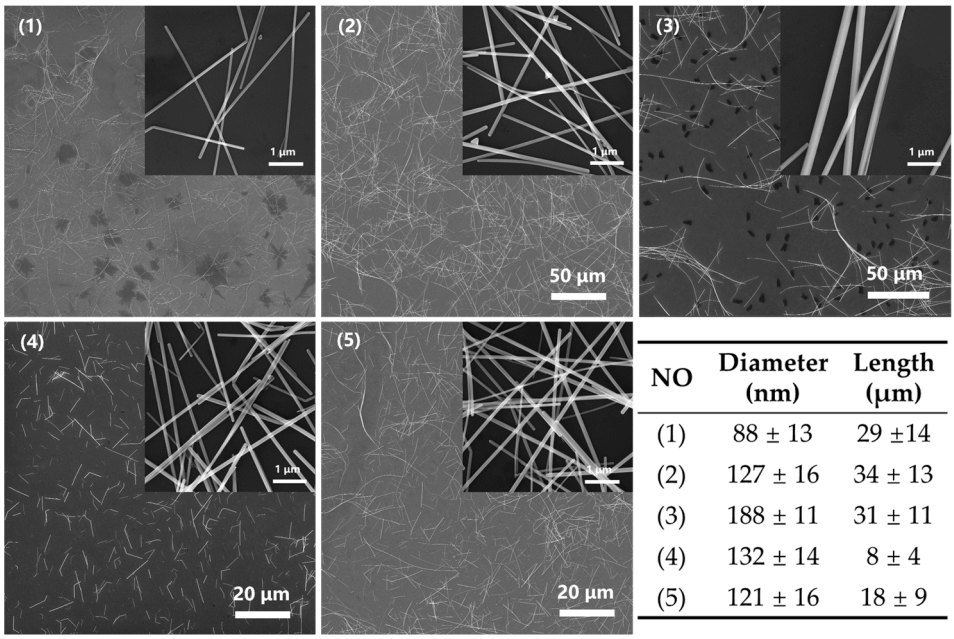

NO	Diameter (nm)	Length (μm)
(1)	88 ± 13	29 ±14
(2)	127 ± 16	34 ± 13
(3)	188 ± 11	31 ± 11
(4)	132 ± 14	8 ± 4
(5)	121 ± 16	18 ± 9

Figure 1. SEM images of five kinds of silver nanowires and their sizes. The scale of each figure in the up-right corner is 1 μm.

Pressure filtration was used to prepare the silver nanowire film. First, water was added to the solution of silver nanowires for dilution, stirred, and washed for 60 min. The dilution ratio was as follows: silver nanowires solution/water = 1:8. Then, the diluent was transferred into the pressure filter through the funnel and the pressure was adjusted to about 0.1 MPa for filtration. The filter paper we used was a PTFE (polytetrafluoroethylene) film with an aperture of 0.3 μm. Finally, the silver nanowire film was peeled and obtained from the filter paper after drying at 80 °C for 6 h.

2.2. Hot-Pressing of Silver Nanowire Films

To evaluate the thermal resistance of silver nanowire film and the shear strength of large-size chip joining, the copper plate/Ag/copper plate sandwiched samples were fabricated by hot press (TY105F-10KN, TIANYU INSTRUMENT, Ningbo, China), as shown in Figure 2. The bonding area was 10 × 10 mm^2, the thickness of each copper plate was 1.6 mm, and the thickness of the silver layer after hot-pressing was about 0.3 mm. In order to prevent the oxidation of the copper plate during hot-pressing, all copper plates were coated with a silver layer of which the thickness was 200 nm. The hot-press sintering process parameters used to prepare all the samples were as follows: the sintering temperature was 250 °C, the bonding pressure was 10 MPa, and the holding time was 10 min in air.

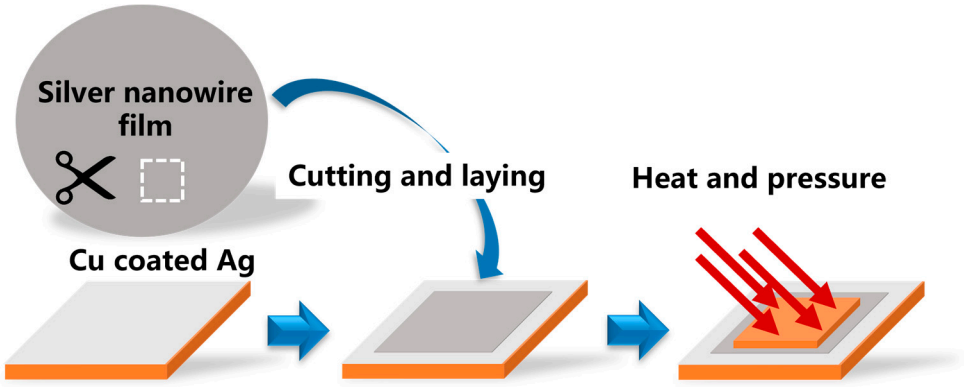

Figure 2. Diagram of hot-pressing of silver nanowire film.

2.3. Characterization Methods

A scanning electron microscope (SEM) (MIRA4 LMH, Tescan, Brno, Czech Republic) was used to observe the micromorphology of silver nanowire film and the section micromorphology of the sandwiched samples. The tensile strength of the silver nanowire film was measured by a tensile tester (Micro 350, Testometrix, Rochdale, UK), and the loading rate of the force was 1 mm/min. A combination of thermogravimetry (TG) and differential scanning calorimetry (STA 449F5, Netzsch, Freistaat Bayern, Germany) was used to characterize the thermal properties of silver nanowire film. The temperature ranged from room temperature to 600 °C in a nitrogen atmosphere, and the heating rate was 10 °C/min.

Thermal resistance is one of the leading performance objectives of silver nanoscale joining materials; it was calculated using the following steps. At first, the thermal conductivity of the sandwich sample was calculated by the equation $\lambda = \alpha \times \rho \times C_p$, where α is the thermal diffusion coefficient of the sandwich sample. It was measured by the laser flash method (LFA 447, Netzsch, Freistaat Bayern, Germany), where ρ is the density of the sandwiched sample, which was measured by the Archimedes drainage method (XS105DU, Mettler Toledo, Zurich, Switzerland), and C_p is the calculated heat capacity. The calculation equation of C_p is $C_p = C_{p,Cu} \times (d_{Cu}/d_{sample}) + C_{p,Ag} \times (d_{Ag}/d_{sample})$, where d is the thickness. $C_{p,Cu}$ and $C_{p,Ag}$ were 0.385 and 0.233 $J \cdot g^{-1} \cdot K^{-1}$, respectively. Although the heat capacity of sintered silver is different from that of bulk silver, the mass of silver in the whole sandwiched sample was only less than 5%, so the equation is considered to be reasonable. Then, we found the thermal resistance of the sandwiched sample through equation $R_{sample} = d_{sample}/\lambda$, and finally obtained the thermal resistance of the joining material through $R_{TIM} = R_{sample} - R_{Cu}$.

Shear strength is another of the leading performance objectives of silver nanoscale joining materials. The schematic diagram of the shear strength measurement of silver nanowire film is shown in Figure 3. We inserted the prepared sample into the mold and used the mechanical testing machine (CMT5000, XINBIAO INSTRUMENT, Shanghai, China) to apply a downward load to test the shear strength of the joint. The loading rate of the force was 0.5 mm/s.

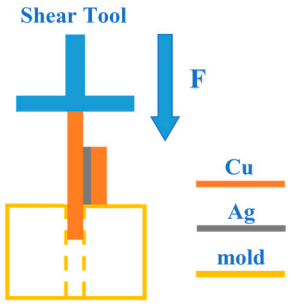

Figure 3. Schematic diagram of shear strength measurement of sandwiched sample.

3. Results and Discussion

3.1. Basic Characteristics of Silver Nanowire Film

Figure 4 shows the silver nanowire film's physical appearance and microscopic morphology. The thickness of silver nanowire film shown in Figure 4a is about 84 μm, but it is not fixed, meaning it can be adjusted by controlling the volume of the silver nanowire solution during pressure filtration. The silver nanoscale joining material, which looks like a sheet, is more suitable for larger-size chip packaging because its area can be adjusted by cutting, while the silver nanoscale paste needs to be dispensed or screen-printed [20]. As can be observed in Figure 4b, the silver nanowires were well-dispersed, and there were many overlap points between the wires, but no coalescence occurred. A good dispersion can effectively avoid the self-sintering of nanowires [20] and prevent the product from failing before use.

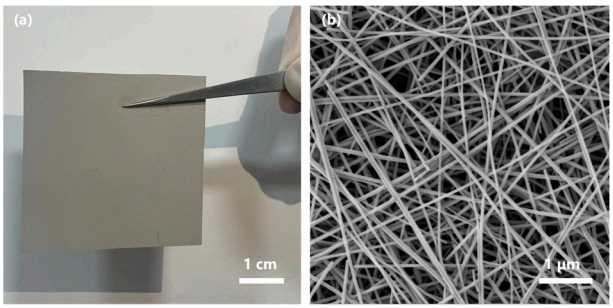

Figure 4. Images of silver nanowire film. (**a**) Physical appearance, (**b**) Microscopic morphology.

The tensile strength of the silver nanowire film was measured by a tensile tester, and the engineering stress –strain curve shows (in Figure 5) that the tensile strength of silver nanowire film is 3.40 MPa, and the strength is derived from silver nanowires. This indicates that the film can be easily cut without shattering. The TG curve of the sample is shown in Figure 6. It can be observed that the mass begins to decrease rapidly near 300 °C, and only 1% mass loss occurs from room temperature to 600 °C. This indicates that the silver content in silver nanowire film is 99.0 wt%, and the mass loss is PVP. The PVP mainly derives from adsorption on the surface during the nucleation and growth of silver nanowires [22]. The low organic content plays an important role in the performance of silver nanowire film. This is because PVP adsorption on the silver nanowire will prevent contact between silver nanowires and thus reduce the sintering driving force. In addition, residual PVP in the sintered silver nanowire film will reduce the thermal conductivity of the sintered silver nanowire film [23].

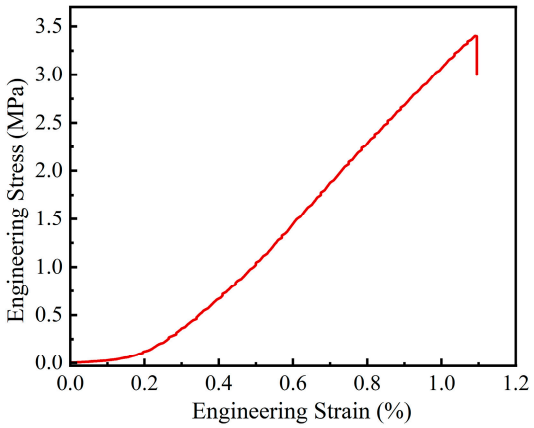

Figure 5. Tensile stress–strain curve of silver nanowire film.

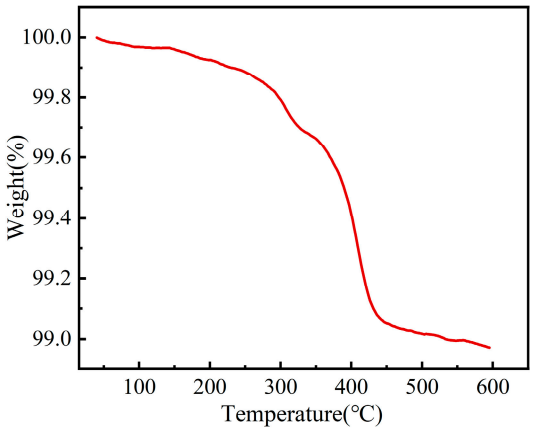

Figure 6. TG curve of silver nanowire film.

In order to investigate the low-temperature sintering characteristics of silver nanowire film, we used DSC for the thermal analysis of silver nanowire film prepared with silver nanowires of different sizes. As shown in Figure 7, the exothermic peaks in the DSC curve are caused by the surface sintering reaction of the silver nanowire (to reduce the surface energy) or the recrystallization of nanowires by heating [24,25], rather than by the decomposition of PVP. This is because all exothermic peaks occurred before PVP decomposition (shown in Figure 6). There is no exothermic peak for PVP decomposition because PVP is of a low content and the decomposition is a slow process.

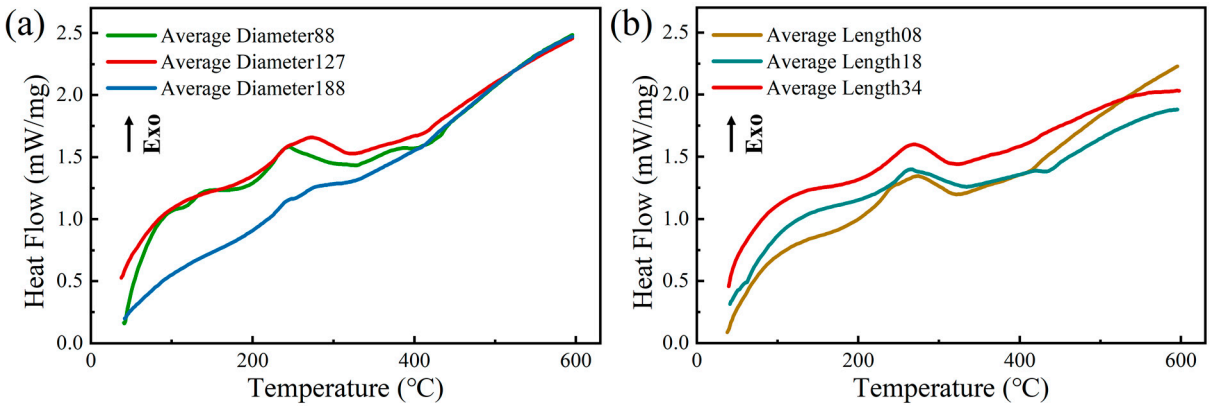

Figure 7. DSC curves of silver nanowire film. (**a**) Silver nanowire films prepared with silver nanowires (1), (2), and (3) in Figure 1. (**b**) Silver nanowire films prepared with silver nanowires (2), (4), and (5) in Figure 1.

Figure 7a is the DSC curve of silver nanowire film prepared with a similar range of lengths but with different diameters of silver nanowires. The figure shows that the silver nanowire film with an average diameter of 88 nm has a significant exothermic peak from 180 °C to 300 °C, while the exothermic peak of the silver nanowire film with an average diameter of 127 nm shifts from 210 to 310 °C. The exothermic peak shifts to a high temperature, and the exothermic heat decreases significantly when the average diameter is 188 nm. It can be explained that the smaller silver nanowire diameter has a lower melting point, and silver nanowires with a lower melting point will recrystallize earlier. So, the exothermic peak gradually shifts to a high temperature with the increase in the diameter of the silver nanowire, while the silver nanowire with an average diameter of 188 nm exhibits an unobvious recrystallization phenomenon [24].

Figure 7b shows the DSC curves of silver nanowire film prepared with a similar range of diameters but with different lengths of silver nanowires. It can be observed from the figure that the exothermic peaks do not change with the change in the length of the silver nanowires, indicating that length is not a factor affecting the low-temperature sintering characteristics of silver nanowire film. The micromorphology images of silver nanowire film sintered at different temperatures in Figure 8 demonstrate this (the samples are from the DSC at different temperatures). From the figure, it can be observed that the linear shape of silver nanowires always exists at low temperatures, while the linear shape of silver nanowires completely disappears at high temperatures (after the exothermic peak). At present, the evolution of the microstructure behavior of silver nanowires during the sintering process is not clear, so further research is needed.

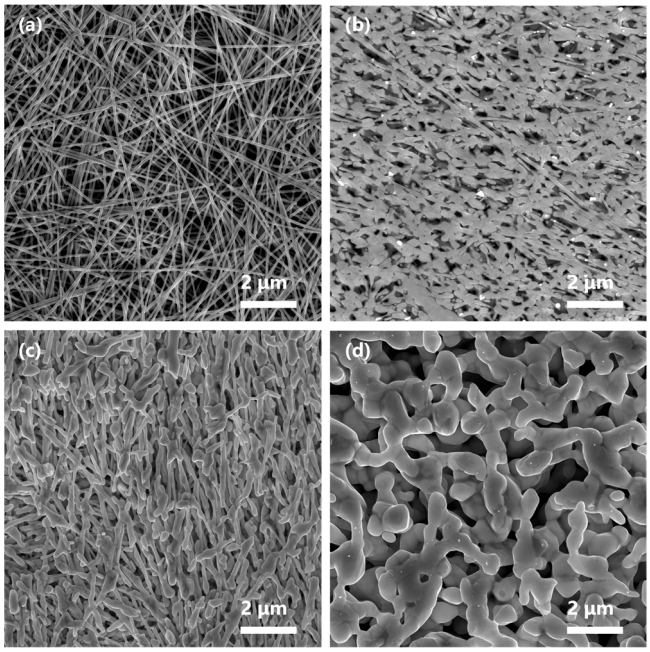

Figure 8. SEM images of silver nanowire film prepared with silver nanowire (1) sintered at different temperatures (**a**) 50 °C, (**b**) 200 °C, (**c**) 250 °C, (**d**) 300 °C.

3.2. Performances of Silver Nanowire Film

Figure 9a is the thermal resistance histogram of sintered silver nanowire film prepared with a range of similar lengths but with different diameters of silver nanowires under the same hot-press condition. The larger diameter generally has a smaller sintering driving force, so the R_{TIM} is higher. However, even the silver nanowires with a diameter of 188 nm have a thermal resistance of only 4.146 $K \cdot W^{-1}$ after sintering, which is lower than the thermal resistance of Pb-Sn solder on the market (the thermal resistance is about 6 $K \cdot W^{-1}$ under the same thickness). This is beneficial due to the ultra-high thermal conductivity of silver, and the sintered silver forms an excellent thermal conduction path between copper plates.

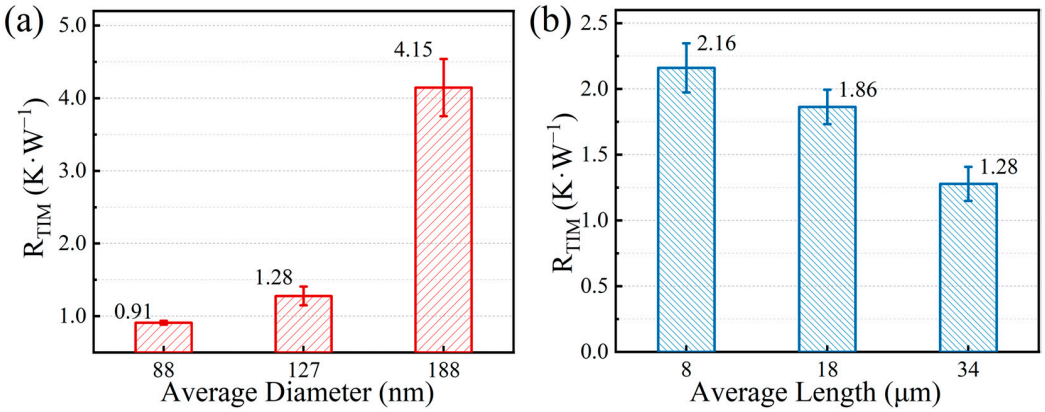

Figure 9. Thermal resistance of sintered silver nanowire film prepared with different sizes of the silver nanowire. (**a**) Silver nanowire films prepared with silver nanowires (1), (2), and (3) in Figure 1. (**b**) Silver nanowire films prepared with silver nanowires (4), (5), and (2) in Figure 1.

Figure 9b is the thermal resistance histogram of sintered silver nanowire film prepared with a range of similar diameters but with different lengths of silver nanowires. The R_{TIM} decreases with the increase in the length of the silver nanowire. To investigate the phenomenon, we observed the cross-sections of the sandwiched samples. As shown in Figure 10, more holes appear with the decrease in the length of the silver nanowire. It can

be explained that the shorter silver nanowire has more cross points, and defects and pores are more likely to form at the cross point during sintering, which results in a higher thermal resistance. In addition, long silver nanowires may have a better thermal conduction path after sintering, which is one of the reasons for their lower thermal resistance compared to short silver nanowires.

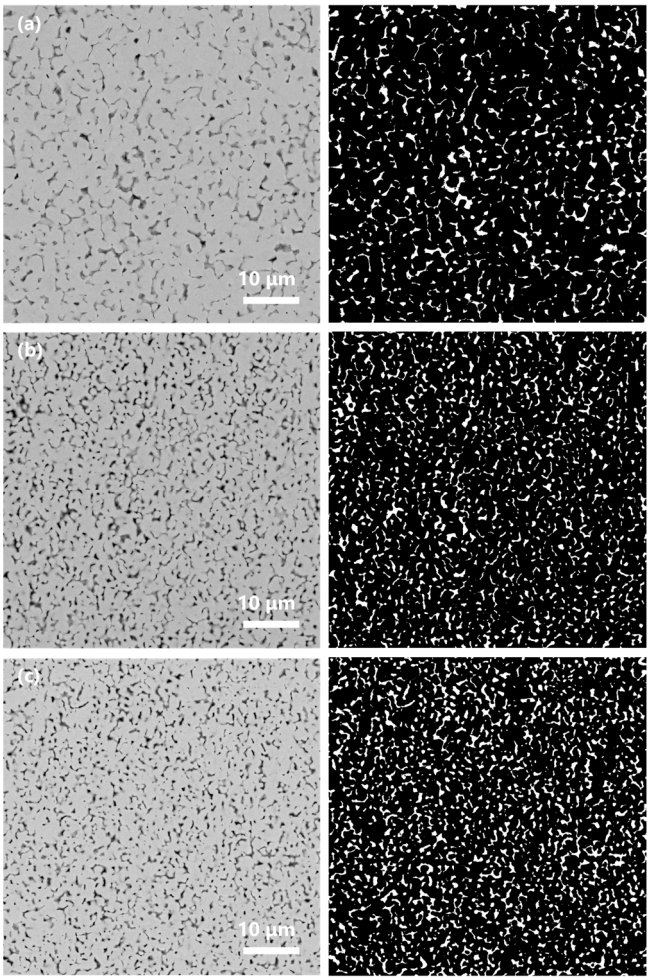

Figure 10. SEM images of cross-sections of the sintered silver nanowire film prepared with similar diameters but different lengths of silver nanowires. The average lengths are (**a**) 34 μm, (**b**) 18 μm, and (**c**) 8 μm, respectively. The images in the right column were reinforced by Image Pro Plus.

As shown in Figure 11a, the shear strength of the joints attached by sintered silver nanowire film prepared with diameters of 88 nm and 127 nm of the silver nanowire is more than 50 MPa, meaning the shear strength of the two joints was close, which indicates that the two kinds of silver nanowires have almost the same degree of sintering. The high strength of 50 MPa can meet the requirements of most electronic packaging. However, the shear strength of joints attached by sintered silver nanowire film prepared with a diameter of the silver nanowire of 188 nm dropped sharply, even lower than that of the Pb-Sn solder (~30 MPa), which may be caused by insufficient sintering. This is consistent with the conclusion of the DSC curve in Figure 7a. Figure 11b is the histogram of the joints attached by sintered silver nanowire film prepared with different lengths of the silver nanowire; the shear strength increases with the increase in the length, indicating that the long silver nanowires after sintering have a more excellent continuity and thus achieve a higher strength, which can be confirmed by the literature [26]. In addition, the variation in the trend of the thermal resistance with the size of silver nanowire is consistent with that of the shear strength. Therefore, it can be concluded that silver nanowire films prepared

from silver nanowires with small diameters and long lengths have better performances after sintering.

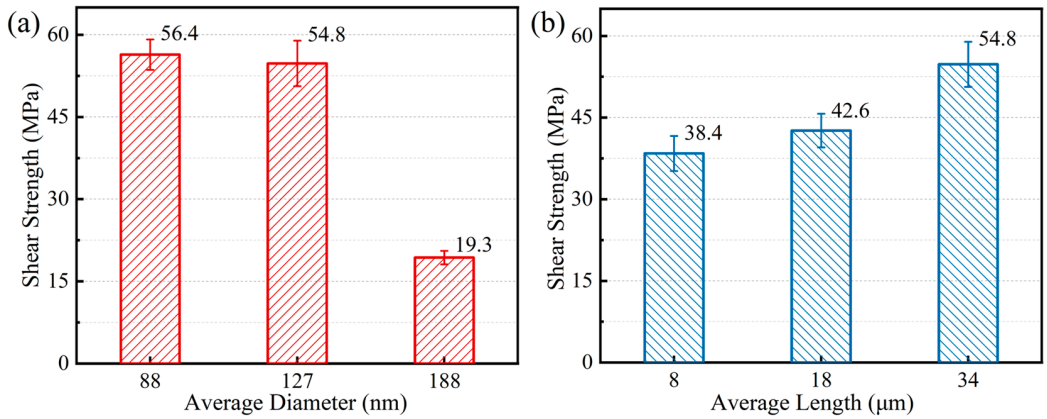

Figure 11. Shear strength of the joints attached by sintered silver nanowire film prepared with different sizes of the silver nanowire. (**a**) Silver nanowire films prepared with silver nanowires (1), (2), and (3) in Figure 1. (**b**) Silver nanowire films prepared with silver nanowires (4), (5), and (2) in Figure 1.

To validate the results above, the fracture of the joints was observed. As a result, two types of fracture were shown in shear experiments. One of the types is shown in Figure 12a—the image shows a porous structure after the sintering of silver nanowires, and there are few traces of plastic deformation. It can be assumed that this type of fracture occurs at the interface between the sintered silver and the copper plate. The shear strength of the joints with such a fracture mode is usually low. The other fracture type is shown in Figure 12b—most areas of the sintered silver nanowire have obvious deformation due to the force, which was mainly manifested by the necking and final fracture of silver grain under the shear stress. This type of fracture occurs in the sintered silver nanowire film itself, and the shear strength of the joints fractured in this way is usually high. In fact, the SEM image of the fracture joint of silver nanowire prepared from silver nanowires with an average diameter of 188 nm after sintering is displayed in Figure 12a, while the other four are outlined in Figure 12b. Figure 13 shows the stress–displacement curves of the two fracture modes in Figure 12. In the curve of high shear strength (red curve), the stress remains almost constant with the increase in displacement, which is a typical performance of material yield. This indicates that the sintered silver nanowire film has good plasticity, which provides good impact and vibration resistance for electronic devices. Thus, the reliability of electronic packaging is greatly enhanced. In contrast, there is no yield phenomenon (shown in the blue curve) for the sintered silver nanowire film that fractured at the interface.

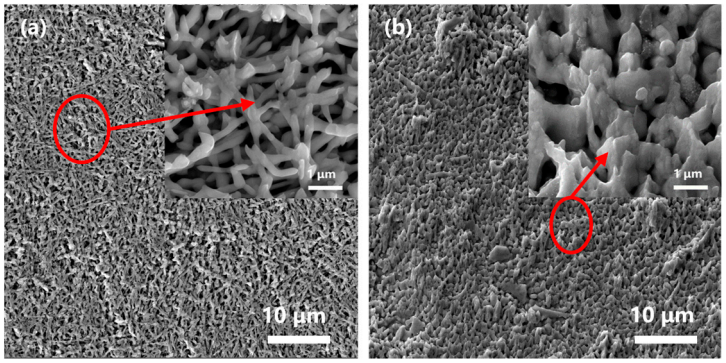

Figure 12. Two typical SEM images of the fracture surface of the joint. (**a**) Fractured at interface, (**b**) Fractured at sintered silver nanowire film. The scale of each figure in the up-right corner is 1 μm.

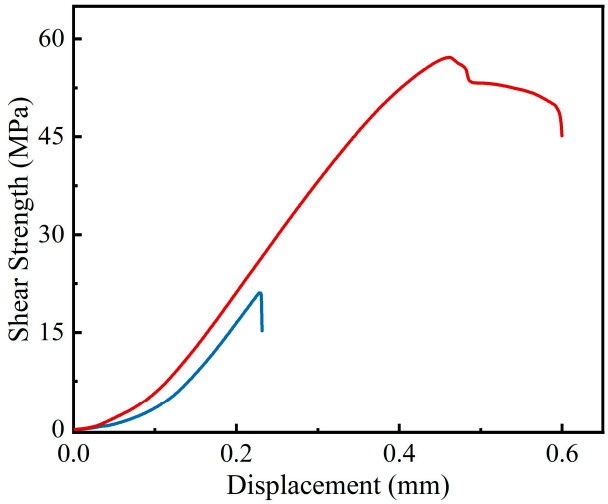

Figure 13. Two typical stress–displacement curves of the joints. Blue line: curve of Figure 12a, red line: curve of Figure 12b.

4. Conclusions

In this study, silver nanowire film was prepared by pressing filtration with silver nanowire, which was synthesized using the polyol method. The film had the characteristics of low-temperature sintering, low organic content, and certain strengths, and its performance was evaluated. The main conclusions are as follows:

(1) The silver nanowire film looks like a sheet, has a tensile strength of up to 3.40 MPa, and the silver content is 99 wt%. The thermal resistance of the sintered silver nanowire film that was hot-pressed at 250 °C 10 MPa was only 1.28 $K \cdot W^{-1}$. The shear strength of the sintered joint was 56.4 MPa, and the fracture occurred in the sintered silver nanowire film and displayed a good plasticity.

(2) Since silver nanowires with a small diameter have a better sintering driving force and longer silver nanowires have fewer holes after sintering, silver nanowire film prepared with smaller-diameter and longer-length silver nanowires has higher thermal conductivity and shear strength after hot-pressing.

Author Contributions: Y.P.: Writing—original draft, investigation, formal analysis; Y.Y.: writing—review and editing, supervision; C.Y.: writing—review and editing. Z.W.: methodology; Y.X.: validation; Y.D.: project administration. All authors have read and agreed to the published version of the manuscript.

Funding: Independent scientific research project of National University of Defense Technology (No. 22-TDRCJH-02-052).

Data Availability Statement: Data are contained within the article.

Conflicts of Interest: The authors declare no conflict of interest.

References

1. Shahzad, D.; Pervaiz, S.; Zaffar, N.A.; Afridi, K.K. GaN-Based High-Power-Density AC-DC-AC Converter for Single-Phase Transformerless Online Uninterruptible Power Supply. *IEEE Trans. Power Electron.* **2021**, *36*, 13968–13984. [CrossRef]
2. Bar-Cohen, A.; Maurer, J.J.; Altman, D.H. Embedded Cooling for Wide Bandgap Power Amplifiers: A Review. *J. Electron. Packag.* **2019**, *141*, 040803. [CrossRef]
3. Li, L.; He, Y.; Wang, L.; Wang, C.; Liu, X. IGBT Lifetime Model Considering Composite Failure Modes. *Mater. Sci. Semicond. Process.* **2022**, *143*, 106529. [CrossRef]
4. Iradukunda, A.-C.; Huitink, D.R.; Luo, F. A Review of Advanced Thermal Management Solutions and the Implications for Integration in High-Voltage Packages. *IEEE J. Emerg. Sel. Top. Power Electron.* **2020**, *8*, 256–271. [CrossRef]
5. Swamy, M.C.K. A Review of the Performance and Characterization of Conventional and Promising Thermal Interface Materials for Electronic Package Applications. *J. Electron. Mater.* **2019**, *48*, 7623–7634. [CrossRef]

6. Huang, Y.; Luo, Y.; Xiao, F.; Liu, B.; Tang, X. Physics of Failure of Die-Attach Joints in IGBTs under Accelerated Aging: Evolution of Micro-Defects in Lead-Free Solder Alloys. *Microelectron. Reliab.* **2020**, *109*, 113637.
7. Wang, X.; Zhang, L.; Li, M. Microstructure and Properties of Sn-Ag and Sn-Sb Lead-Free Solders in Electronics Packaging: A Review. *J. Mater. Sci. Mater. Electron.* **2022**, *33*, 2259–2292. [CrossRef]
8. Cheng, S.; Huang, C.-M.; Pecht, M. A Review of Lead-Free Solders for Electronics Applications. *Microelectron. Reliab.* **2017**, *75*, 77–95. [CrossRef]
9. Yan, J. A Review of Sintering-Bonding Technology Using Ag Nanoparticles for Electronic Packaging. *Nanomaterials* **2021**, *11*, 927. [CrossRef]
10. Lederer, M.; Gokdeniz, Z.; Khatibi, G.; Nicolics, J. Constitutive Equations for Strain Rate and Temperature Dependent Mechanical Behaviour of Porous Ag-Sintered Joints in Electronic Packages. *Microelectron. Reliab.* **2021**, *126*, 114209. [CrossRef]
11. Yan, J.; Zou, G.; Liu, L.; Zhang, D.; Bai, H.; Wu, A.; Zhou, Y.N. Sintering Mechanisms and Mechanical Properties of Joints Bonded Using Silver Nanoparticles for Electronic Packaging Applications. *Weld. World* **2015**, *59*, 427–432. [CrossRef]
12. Fan, J.; Xu, D.; Zhang, H.; Qian, C.; Fan, X.; Zhang, G. Experimental Investigation on the Sintering Kinetics of Nanosilver Particles Used in High-Power Electronic Packaging. *IEEE Trans. Compon. Pack. Manuf. Technol.* **2020**, *10*, 1101–1109. [CrossRef]
13. Hsu, S.L.-C.; Chen, Y.-T.; Chen, M.-L.; Chen, I.-G. Low Sintering Temperature Nano-Silver Pastes with High Bonding Strength by Adding Silver 2-Ethylhexanoate. *Materials* **2021**, *14*, 5941. [CrossRef]
14. Kim, Y.-J.; Park, B.-H.; Hyun, S.-K.; Nishikawa, H. The Influence of Porosity and Pore Shape on the Thermal Conductivity of Silver Sintered Joint for Die Attach. *Mater. Today Commun.* **2021**, *29*, 102772. [CrossRef]
15. Zhang, H.-Q.; Bai, H.-L.; Jia, Q.; Guo, W.; Liu, L.; Zou, G.-S. High Electrical and Thermal Conductivity of Nano-Ag Paste for Power Electronic Applications. *Acta Metall. Sin. Engl. Lett.* **2020**, *33*, 1543–1555. [CrossRef]
16. Lei, T.G.; Calata, J.N.; Lu, G.-Q.; Chen, X.; Luo, S. Low-Temperature Sintering of Nanoscale Silver Paste for Attaching Large-Area (>100 mm^2) Chips. *IEEE Trans. Compon. Packag. Technol.* **2010**, *33*, 98–104. [CrossRef]
17. Wang, C.; Li, G.; Xu, L.; Li, J.; Zhang, D.; Zhao, T.; Sun, R.; Zhu, P. Low Temperature Sintered Silver Nanoflake Paste for Power Device Packaging and Its Anisotropic Sintering Mechanism. *ACS Appl. Electron. Mater.* **2021**, *3*, 5365–5373. [CrossRef]
18. Shen, X.; Li, J.; Xi, S. High Strength Die-Attach Joint Formation by Pressureless Sintering of Organic Amine Modified Ag Nanoparticle Paste. *Nanomaterials* **2022**, *12*, 3351. [CrossRef]
19. Yang, D.; Huang, Y.; Tian, Y. Microstructure of Ag Nano Paste Joint and Its Influence on Reliability. *Crystals* **2021**, *11*, 1537. [CrossRef]
20. Siow, K.S. Mechanical Properties of Nano-Silver Joints as Die Attach Materials. *J. Alloy. Compd.* **2012**, *514*, 6–19. [CrossRef]
21. Paknejad, S.A.; Mannan, S.H. Review of Silver Nanoparticle Based Die Attach Materials for High Power/Temperature Applications. *Microelectron. Reliab.* **2017**, *70*, 1–11. [CrossRef]
22. Xia, Y.; Xiong, Y.; Lim, B.; Skrabalak, S.E. Shape-Controlled Synthesis of Metal Nanocrystals: Simple Chemistry Meets Complex Physics? *Angew. Chem. Int. Ed.* **2009**, *48*, 60–103. [CrossRef]
23. Yan, J.; Zou, G.; Wu, A.; Ren, J.; Yan, J.; Hu, A.; Zhou, Y. Pressureless Bonding Process Using Ag Nanoparticle Paste for Flexible Electronics Packaging. *Scr. Mater.* **2012**, *66*, 582–585. [CrossRef]
24. Yu, H.; Li, L.; Zhang, Y. Silver Nanoparticle-Based Thermal Interface Materials with Ultra-Low Thermal Resistance for Power Electronics Applications. *Scr. Mater.* **2012**, *66*, 931–934. [CrossRef]
25. Moon, K.-S.; Dong, H.; Maric, R.; Pothukuchi, S.; Hunt, A.; Li, Y.; Wong, C.P. Thermal Behavior of Silver Nanoparticles for Low-Temperature Interconnect Applications. *J. Electron. Mater.* **2005**, *34*, 168–175. [CrossRef]
26. Guo, W.; Zhang, H.; Zhang, X.; Liu, L.; Peng, P.; Zou, G.; Zhou, Y.N. Preparation of Nanoparticle and Nanowire Mixed Pastes and Their Low Temperature Sintering. *J. Alloy. Compd.* **2017**, *690*, 86–94. [CrossRef]